Bull. Astr. Soc. India (2002) 30, 291–296

Observations of Markarian 421 by the CAT imaging telescope

P.Fleury

IN2P3 / Ecole Polytechnique, 91128 Palaiseau

Abstract.
The CAT imaging telescope has been exploited since 1997 for the observation of Mrk-421 among other sources. After a brief review of thecharacteristics of the CAT telescope, the event reconstruction method will be described. We then present recent analysis results, with emphasis on the determination of the energy spectrum, its shape and its dependence upon the level of activity of the blazar.

Key words: Gamma Astronomy, Space Astronomy, Atmospheric Cherenkov Detectors

1. Introduction

The CAT telescope consists of a $17m^2$ reflector with a 600 pixel camera. Due to a large focal length ($F/D \approx 1$) and good quality mirror elements, the aberrations are less than 2 arcmin and the isochronism is better than 1 ns. This is exploited by the use of a fast trigger (2ns) and a short integration time (8 ns). This also allows fine imaging with pixel sizes as small as 0.13^o in diameter (apart from a guard ring with four times larger pixels). On the basis of our personal experience with the Whipple 10m telescope, we aimed at minimising the number of photoelectrons necessary for the reconstruction of shower images, so as to reach about the same energy threshold ($\approx 250GeV$) with a four times smaller reflector area (Barrau, 1998).

A further advantage of the fine pixel resolution is that the profile of a shower image, in length and width, can be better analysed, allowing in particular the differentiation of the top of the shower from its lower part. Each recorded image is checked against a series of pre-established templates representing showers of different energies and different impact distances for a range of different source directions. With just a single telescope, the stereoscopic determination of each shower can be reconstructed, and its source position can be determined. This stereoscopic reconstruction of CAT images was implemented with success by S.Lebohec (Ref Le Bolec 1998) and is commonly used in our analysis.

Most of the γ-events collected with CAT resulted from the observation of the Crab nebula and of Mrk-421 and Mrk-501. Many other sources have been observed with no significant signal at present (that is, above 5 σ significance). In section 2, the data from Mrk-421 will be shown and its reduction discussed. The extraction of the energy distribution will be presented in section 3 and, in section 4, we shall comment on the spectrum so obtained.

2 Data from the CAT telescope

The data obtained by CAT for Mrk-421 ON and OFF source observations are shown in Fig.1 for the very high flare of the night of 04-05 February, 2000. The first inset (on the left) is the subtraction ON-OFF: the γ signal is clearly seen in the first bins. On these plots, the α parameter is used as usual to evaluate the good alignment of the shower image with respect to the pointing position (assumed to coincide with the source). But, the scale of α now extends over a domain 180^o instead of 90^o, because the image has gained a top to bottom orientation thanks to the template analysis.

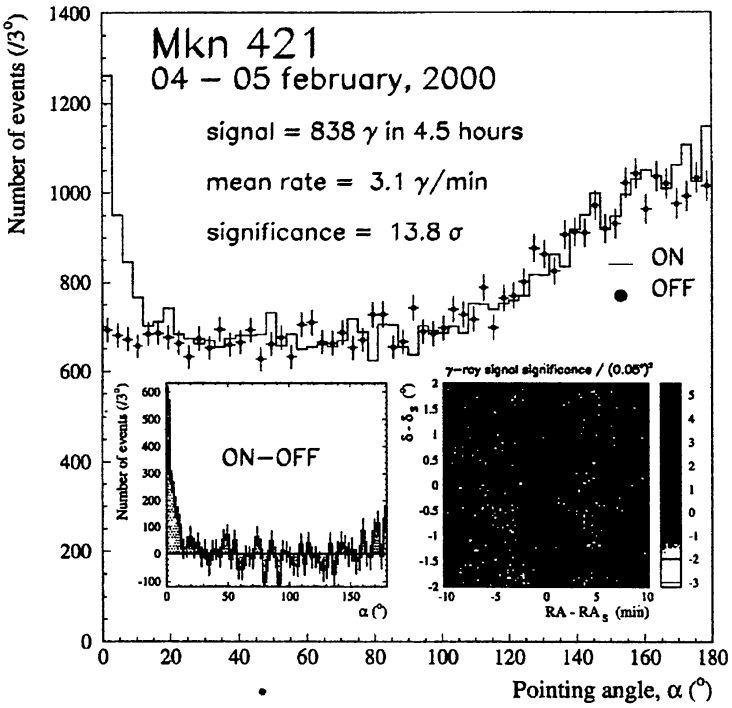

Figure 1. The α alignment angle from the observation of Mrk-421 for the night of 04-05 February 2000. Left inlet, the $[0^o - 180^o]\alpha$ distribution for the ON-OFF subtraction. Right inlet, the field of view of the reconstructed source points.

To clarify further this peculiarity of the CAT template method, we show in Fig.2 a set of longitudinal and transverse projections of the templates relative to showers of 1 TeV energy falling at several impact distances from the telescope axis. The longitudinal projections clearly display a top/down assymetry which is exploited by our analysis to differentiate the shower propagation direction along each particular image.

Furthermore, the longitudinal deployment of the shower can be extrapolated upwards, to infinity in real space, that is to the point source in the camera field of view. This point is represented by a star on the longitudinal plot, in Fig.2. It is located at the origin of the longitudinal axis since it constitutes here the reference point for the longitudinal distribution. In the fitting procedure, for each event, the source coordinates are left as free parameters, to be determined by the fitting procedure.

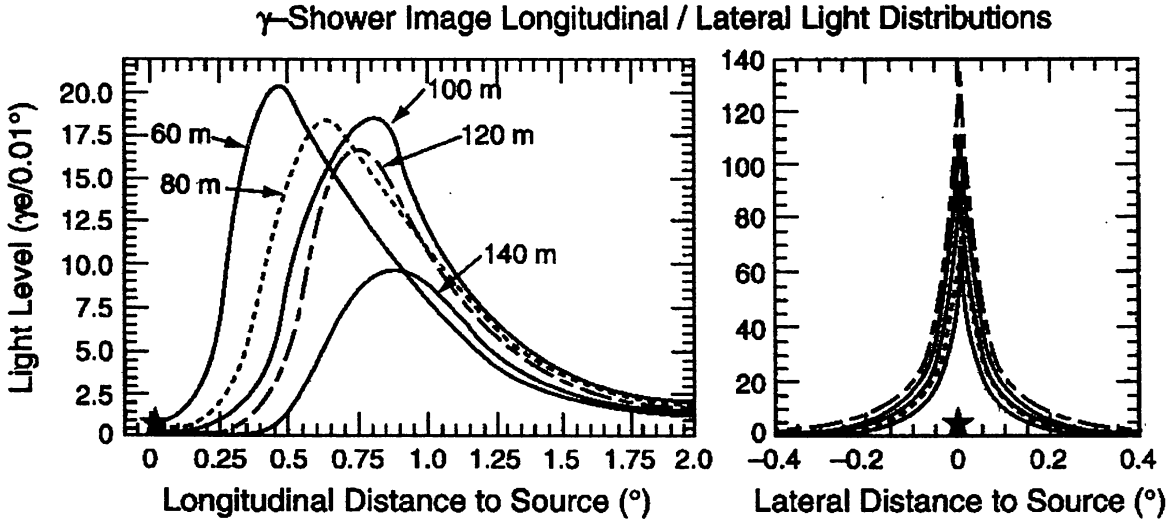

Figure 2. The templates : longitudinal and transverse projections of shower images (LeBohec 1998).

This event by event determination of the point source is used to establish the two-dimensional map shown in the second insert on the right side of Fig.1. This is a map of significance of event excess per bin of 0.05^o: the source lies at the centre and the axis gives the difference in right ascension and declination with respect to the source co-ordinates. The angular resolution per event is found to be 0.11^o allowing source location determination with an accuracy better than 1' (systematic dominated).

3 Energy distribution of Mrk-421

Due to the energy uncertainties and to the steep energy distribution (according to $\approx E^{-3}$), care must be taken about accidental transfers of events from energy bin to energy bin which are dependent upon the energy distribution itself.

Two hypotheses are considered, H_0 and H_1:

- H_0 : $\phi_o E^{\gamma}$, a simple power law :
- H_1 : $\phi_o E^{-\gamma-\beta log E^{\gamma}}$, or a modified power law to include an effect of curvature.

In a log-log plot, these distributions are represented respectively

- according to a straight line : $log\phi = log\phi_o - \gamma logE$
- according to a parabola : $log\phi = log\phi_o - \gamma logE - \beta log^2 E$

This modified power law, with a second order term in $logE$, has been previously used by the Whipple group for the study of Mrk501 (Ref Krennrich 1999).

According to the method usually found in the literature, (e.g. Aharonian 1999), the power law or modified power law coefficients, ϕ_o, γ and β, are obtained by a χ^2 procedure, fitting energy bin by energy bin the number of source events, - the difference between ON and OFF source observations for each bin - against the expected number of events given a set of effective detection areas established for each energy bin. As this MonteCarlo evaluation of the bin by bin effective area depends on the flux distribution, its determination is necessarily an iterative procedure.

Instead, we have chosen a maximum likelihood method, starting with the observed population per bin, ON and OFF independently, as well as the assumed expressions for the spectral law, plus the knowledge of the detector response (γ-ray effective area per bin, and energy resolution). This method directly provides the only relevant physical results, that is the most probable spectral parameters and their covariant matrix.

To establish the relevance of the curvature parameter, the likelihood ratio λ of the two different analytical hypothesis H_o and H_1 is used: $\lambda = -2[logL(H_o)/L(H_1)]$ which behaves like a χ^2 distribution for one degree of freedom.

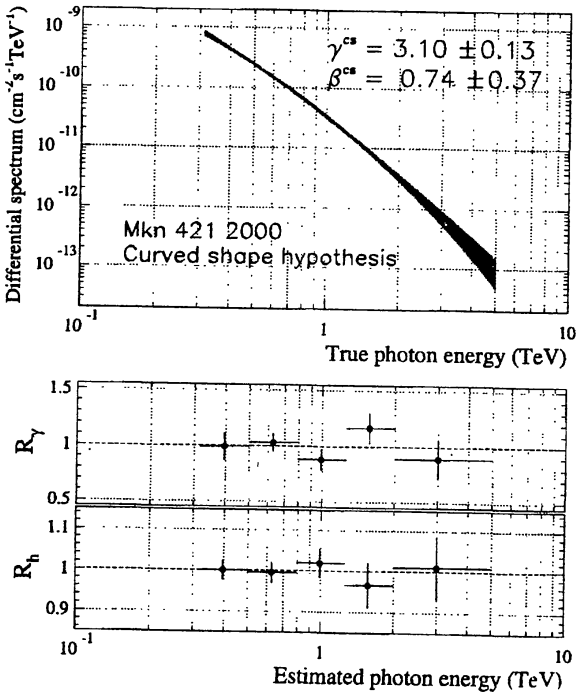

Figure 3 Mrk-421 flare of the night 4-5 Feb 2000 : the modified power law and its fitted parameters $\phi = 3.34 \pm 0.28, \gamma = 3.10 \pm 0.13$ and $\beta = 0.74 \pm 0.37$ (Piron 2001).

Due to this rather unusual procedure the results are presented in an unusual way in Fig.3. For a given hypothesis, instead of the most probable curve we chose to show the 68% probability level contours. Furthermore, as we did not need to apply bin by bin corrections on the data, it would not make much sense to show corrected data for

each bin, along the curve. It is more relevant to show, as in the lower parts of Fig.3, independently for the ON and OFF data and for each energy bin, the difference between the observed number of events and the number expected for the optimal distribution law.

4. Results and discussions

To comment on the results, it is convenient to switch from the differential flux distribution $d\phi/dE$ to the SED, the Spectral Energy Distribution, which is deduced from the former by a factor E^2 which flattens out the steep power law. The SED corresponds also to the energy flux per intervals of logE ($SED = E^2 d\phi/dE = Ed\phi/dlogE$).

On the SED log/log plot, the power law and the modified power law preserve their genuine representation of respectively a straight line and a parabola :

- $log\phi = log\phi_o - \gamma logE$ becomes $logSED = log\phi_o - (\gamma - 2)logE$
- $log\phi = log\phi_o - \gamma logE - \beta log^2 E$ becomes $logSED = log\phi_o - (\gamma - 2)logE - \beta log^2 E$

where the modification from $d\phi/dE$ to SED is simply the replacement of γ by $(\gamma - 2)$.

As a result, the slope of the power law is less, and the curved part of the parabola is now within the region of interest :

$logE_{max-\phi} = -(\gamma)/2\beta$ becomes $logE_{max-SED} = -(\gamma - 2)/2\beta$,

that is, the transformation of $d\phi/dE$ to SED has brought the point of turnover closer to the high energy region by a factor $10^{1/\beta}$. With SED, the comparison of Mrk-421 and Mrk-501 becomes quite interesting, as shown in Fig.4.

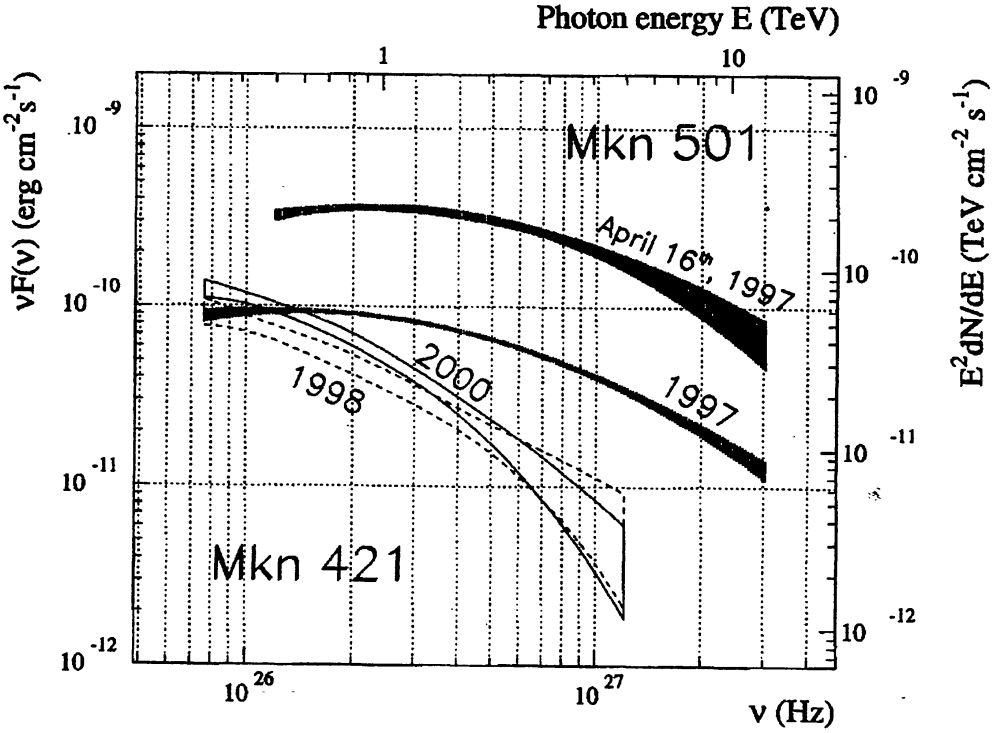

Figure 4. The SED log/log plot for a few flaring periods of Mrkn-421 and Mrk-501. The maximum (or turnover energy) is within the observation region for Mrk-501, and quite significantly below for Mrk-421.

The SED of Mrk-501 has its inverse Compton peak maximum within the Cherenkov energy domain (e.g. Djannati 1999), and the position of this maximum moved to even higher energies during the intense flare of 1997, simultaneously with a hardening in the X-ray emission as observed by Beppo-SAX.

Comparing Mrk-421 present data with the Mrk-501 as shown in Fig 4, we observe that Mrk-421 spectrum hardly reaches energies as high as Mrk-501. Assuming that the overall shape is alike for both apart from two scale factors, in energy and intensity, then we understand that it is more difficult to establish the existence of a turnover for Mrk-421 : the turnover of its SED plot remains below the observed energy region. Mrk-421 seems to follow the same sort of energy drift as Mrk-501 during flares, as shown by the spectrum of Feb 2000 which displays more curvature.

Attempting one step further, as the curvature term, for the flaring Mrk-421, $\beta \approx 0.75 \pm 0.37$, is reasonably close to well measured for the flare of Mrk-501 (Djannati 1999), $\beta = 0.50 \pm 0.07$, we may assume that both of them constitute a realistic base for the extrapolation to their respective turnover energies. Very tentatively, we quote numbers with no error bars of ≈ 0.2 and $1TeV$ for the flaring Mrk-421 and Mrk-501 respectively. This would give a factor ≈ 5 in between their respective energy scales.

5. Conclusion

A very similar mechanism seems to rule the transient behaviours of both Mrk-421 and Mrk-501. The energy spectrum could be described as the fall-off of a 'inverse Compton' bump, whose energy at its maximum increases during flares. This common variability pleads in favour of an imprint of the acceleration mechanism in the jet and would have nothing to do with absorption of TeV-γ-rays by the infrared diffuse light.

References

Aharonian, F.A. A&A **349** (1998) 11

Barrau A., et al. NIM **A416**(1998) 278-292

Djannati-Attai A. et al. *Very high γ-ray spectral properites of Mrk 501 from CAT Chérnkov telescope observations in 1997* A&A **350** (1999) 17-24

Krennrich F., et al. ApJ **511** (1999) 149

Le Bohec S., et al. NIM **A416**(1998) 425-437

Piron F. et al. *Temporal and spectral gamma ray properties of Mrk-421 above 25O GeV from CAY observations between 1996 and 2000* A&A (2001) acccepted